Indian Journal of Engineering & Materials Sciences
Vol. 30, June 2023, pp. 490-494
DOI: 10.56042/ijems.v30i3.3713

Opto-structural Properties of Thermally Treated Zirconia Nanoparticles

Saruchi Rani, Surbhi Verma, & Sushil Kumar*

Department of Physics, Chaudhary Devi Lal University, Sirsa 125 055, India

Received: 10 May 2023; Accepted: 31 May 2023

In this study, zirconia nanoparticles wereprepared throughsol–gel/ spin coating technique using zirconium oxychloride octahydrate as precursor. The prepared gels/thin films were dried at 100 ^{0}C for 24h. Powdered samples and thin films of ZrO_2were heat treated at 550 and 850 ^{0}C for 3h. Structural, microstructural, optical, luminescent and thermal properties of synthesized samples were investigated by X-ray diffraction, Fourier transform infrared spectroscopy, Raman spectroscopy, Scanning electron microscopy, Energy dispersive X-ray spectroscopy, Ultraviolet–visible spectroscopy, Photoluminescence spectroscopy and Thermo-gravimetric analysis. XRD, FTIR and Raman spectroscopies confirmed the presence of both phases i.e tetragonal as well as monoclinic in the prepared samples. Optical band gap of prepared thin films was increased with thermal treatment. PL results revealed a broad band obtained in blue region of EM spectra. Thermal decomposition confirmed the formation of crystalline zirconia nanoparticles.

Keywords: Zirconia, Sol-gel, Spin coating, Annealing, Structural parameters, Optical parameters

1 Introduction

As nanotechnology works on the level where atomic and molecular interactions occur, it becomes a great area of interest by which one can get desired product by manipulating atoms/molecules similar to that of biotechnology. Metal oxides have a large range of electro-chemical properties, so they have an enormous area of interest in research and technological applications in chemistry, physics, materials science etc. Oxides bear a wide range in the band gap which leads to their metallic, semiconducting, insulating and superconducting nature. They exhibit diversified behavior due to specific difference in their electronic structure. These properties make them a great area of interest for research, and they have applications in making microelectronic devices[1], sensors[2], fuel cells[3], coatings[4], catalysts[5], optoelectronic devices[6], etc.

Zirconium dioxide (ZrO_2) is a technologically important material, as it can be used as a solid electrolyte, as a structural ceramic, as a catalyst, as a gas sensor and many more[7-11]. Physico-chemical properties of particle changes due to modifications in structural or electronic energy levels when zirconia based particles size reduced from bulk to nano, and due to thermal treatment. Generally, tetragonal-monoclinic transformation in nanosized pure zirconia is favored on increasing annealing temperature[12].

*Corresponding author (E-mail: sushil.phys@gmail.com)

In the present research work, sol-gel wet chemical method has been used for the synthesis of samples in powder form and spin coating technique has been used for deposition of thin films on glass substrates. The complementary techniques have been employed for characterization of prepared samples.

2 Materials and Methods

2.1 Synthesis

Transparent nanocrystalline zirconia nanopowders/ thin films were prepared by sol–gel/ spin coating technique using zirconium oxychloride octahydrate as source material. Synthesis route for the preparation of powdered samples as well as thin films of zirconia (ZrO_2)are elucidated in Fig. 1

2.2 Characterization

Characterization techniques used to analyze the properties of zirconia (powders as well as thin films) annealed at different temperatures are listed in Table 1.

3 Results and Discussion

3.1 XRD analysis

XRD patterns of pure zirconiathermally treated at 550 and 850 ^{o}C are depicted in Fig. 2. Existence of crystalline phases such as monoclinic and tetragonal is revealed by XRD.

Bragg reflections corresponding to tetragonal phase (t) are located at 30.2^o(111), 34.8^o (200), 50.1^o (220)

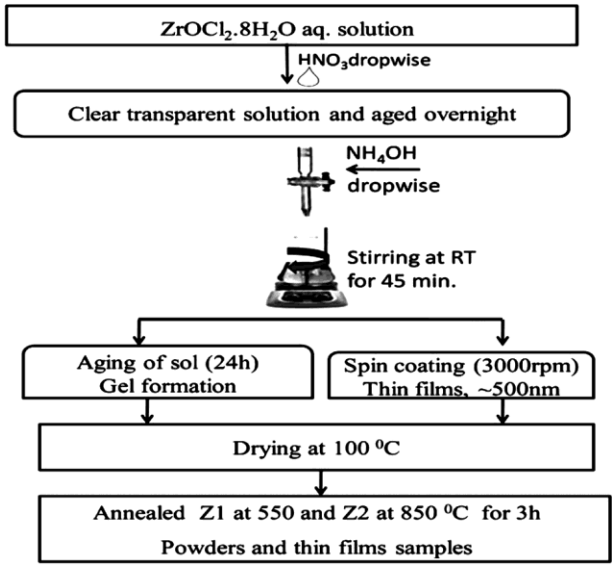

Fig. 1 — Flow chart for the synthesis of zirconia nanopowders/thin films annealed at different temperatures.

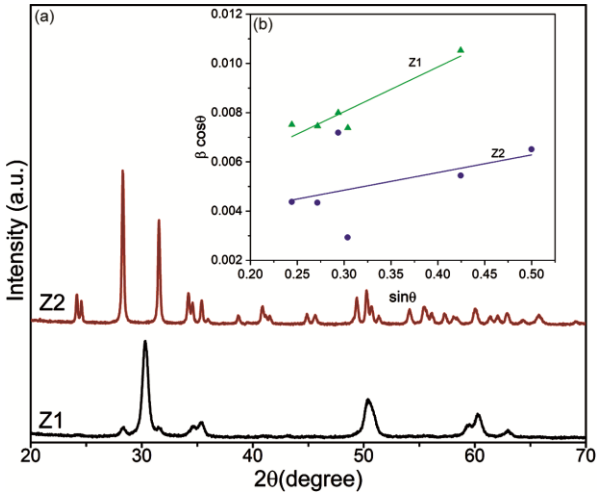

Fig. 2 — (a) XRD patterns, and (b) W-H plots for zirconia nanopowders annealed at different temperatures.

and 59.3°(311) (t-ZrO_2, JCPDS card no.17-0923). Diffraction peaks centered at 24.1°, 28.2°, 31.3°, 34.9°,50.3° and 59.1° corresponding to planes (110), (-111), (111),(200), (220) and (131) respectively are assigned to monoclinic phase (m-ZrO_2, 03-065-2357)[13]. These results are almost similar to the results of our earlier publications[14]. Peaks at~50.2° and 59.3° show mixed phase of monoclinic as well as tetragonal which are in well consistence with the results reported by S. Jayakumar[15].

From Fig. 2, it has been observed that assamples are heated thermally from 550 to 850 °C, tetragonal phase observed at 30.3^0 has been completely disappeared; while the characteristic peaks of monoclinic phase at 28.2^0 (-111) and 31.4^0 (111) [ICDD No. 37-1484] became predominant, in addition to the development of other peaks of monoclinic phase as shown in Fig. 2.

Table 1 — Characterization techniques used to analyze the properties of zirconia nanopowders/thin films annealed at different temperatures

Properties	Techniques used	Range of measurements	Instrument used
Structural	XRD	20-70°	X'Pert-Philips
	FTIR	400-4000 cm^{-1}	Perkin-Elmer 1600
	Raman	75-750 nm	RFT-6000 FT-RAMAN
Microstructural	SEM EDX	Scale 300 μm Element At (%)	JEOL/EO, version 1.0
Thermal	TGA	RT-990 °C	Perkin Elmer, STA 6000
Optical	UV-visible	200-800 nm	Comspec M550
	PL	350-600 nm	Perkin Elmer, LS-50B

The crystallite size, microstrain, lattice parameter and texture coefficient (TC) are evaluated by following relations and values are depicted in Table 2:

$$D = \frac{k\lambda}{\beta cos\theta} \quad \ldots(1)^{16}$$

$$\beta cos\theta = \frac{k\lambda}{D} + \eta sin\theta \quad \ldots(2)^{17}$$

$$\frac{1}{d^2} = \frac{h^2+k^2}{a^2} + \frac{l^2}{c^2} \quad \ldots(3)$$

$$V = a^2c \quad \ldots(4)$$

$$TC_{(hkl)} = \frac{I_{hkl}}{I^o_{hkl}} / \frac{1}{n}\sum\frac{I_{hkl}}{I^o_{hkl}} \quad \ldots(5)$$

The symbols used in above equations have their usual meaning. Texture coefficient (TC) having value greater than 1 is assumed to be preferred orientation. In our study, it has been observed that at temperature 850 °C preferred orientation is along plane (-111) followed by (200). Due to preferred orientation and recrystallization, crystallite size increases and microstrain decreases with temperature[18].

3.2 FTIR analysis

Figure 3 shows FTIR spectra of heat treated zirconia in wavenumber range of 400-4000 cm^{-1}.

Table 2 — Structural parameters of zirconia nanopowders annealed at different temperatures.

Annealing Temperature (^{O}C)	Crystallite Size D (nm)		Lattice Constant (Å)		Unit cell volume V (Å^3)	Dislocation Density $\delta = 1/D^2$ (10^3 nm^{-2})	Micro-strain η	Texture coefficient (TC)
	D-S	W-H	a	c				
550	13.38	20.68	3.599	5.258	68.106	2.34	0.007	0.94 (-111) 0.89 (200)
850	37.60	48.25	3.587	5.247	67.511	0.43	0.003	1.13 (-111) 1.01 (200)

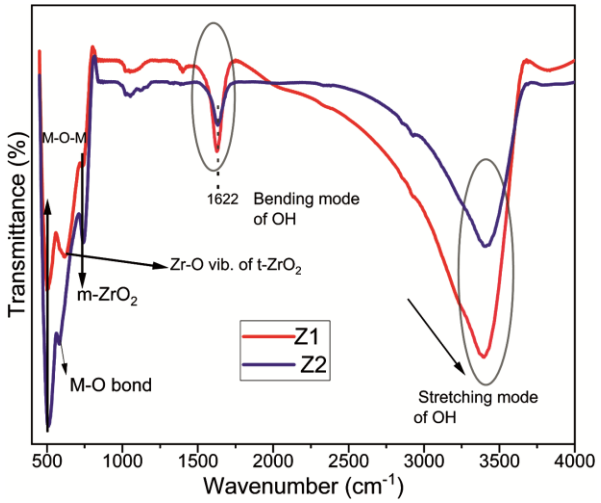

Fig. 3 — FTIR spectra of zirconia nanopowders annealed at different temperatures.

FTIR spectroscopy gives information about molecular structure, functional group and chemical bonding present in a sample. Two bands have been observed at 380-3420 and 1622 cm^{-1}, which may be due to stretching mode and bending mode of –OH bond respectively. In sample Z1, a peak centered at 620 cm^{-1} is assigned to Zr-O vibration of t-ZrO_2 [15]. Metal-oxygen-metal (Zr-O-Zr) and metal-oxygen (Zr-O) bonding corresponding to 501cm^{-1} and 573 cm^{-1}respectively have been observed. Small peaks at 735 cm^{-1} in sample Z1 and at 745 cm^{-1} in sample Z2, are ascribed to m-ZrO_2. The peak becomes more intense as temperature increases from 550 to 850 ^{o}C i.e. monoclinic phase tends to dominate with rise in temperature. Results of FTIR are corroborated with the findings of XRD.

3.3 SEM and EDX

Surface morphology and elemental composition of all the samples were estimated by scanning electron microscopy and energy dispersive X-ray spectroscopy. SEM micrographs exhibit that the samples are porous in nature and have irregular tetragonal structure as shown in Fig. 4(a) The elemental composition of pure ZrO_2 has been evaluated from EDX spectra (Fig. 4(b)) exhibiting the peaks of O and Zr elements. Zr and O are present very nearly in stoichiometric ratio. No other peaks of impurities have been detected.

3.4 Raman analysis

To distinguish the crystalline phases present in samples, Raman spectroscopy has been widely used. Raman spectra corresponding to sample Z2 is depicted in Fig. 4(c).In case of zirconia,

18 ($9A_g$ +9 B_g) modes of monoclinic phase and 6 (A_{1g}+ $2B_{1g}$+$3E_g$) modes of tetragonal phase have been predicted by the factor group analysis. Whereas in our study, 14 ($8A_g$+$6B_g$) active modes corresponding to monoclinic phase and 2 ($2E_g$) modes corresponding to tertragoanl phase of zirconia have been observed and are depicted in Fig. 4(c) and Table 3. Further, the active vibrational modes correspondingto 476 and 640 cm^{-1}can be assigned to both tetragonal and monoclinc phasesof zirconia[15], which are in reasonably agreement with the results of XRD.

3.5 Thermal studies

In order to understand the changes occurred after removal of surface impurities, thermal decomposition process has been employed. Figure 4(d) shows a total weight loss of about ~ 52%. During thermal process, the first stage weight loss~10 % in range 20-250 0C, assigned to the removal of water/impurities from prepared zirconia nanoparticles, and the second stage weight loss ~ 42% in 250-500 ^{0}C range, may be due to removal of NH_4Cl. Beyond 500 ^{0}C, the formation of crystalline phase took place, as confirmed from the results of XRD also.

3.6 UV-visible analysis

The UV-visible absorption spectra of prepared thin films (Fig. 5) was recorded in 200–800 nm region using Comspec M550 spectrophotometer. To investigate the temperature effect on optical absorption and band gap of thin films, the absorption spectra were evaluated. It showed continuous

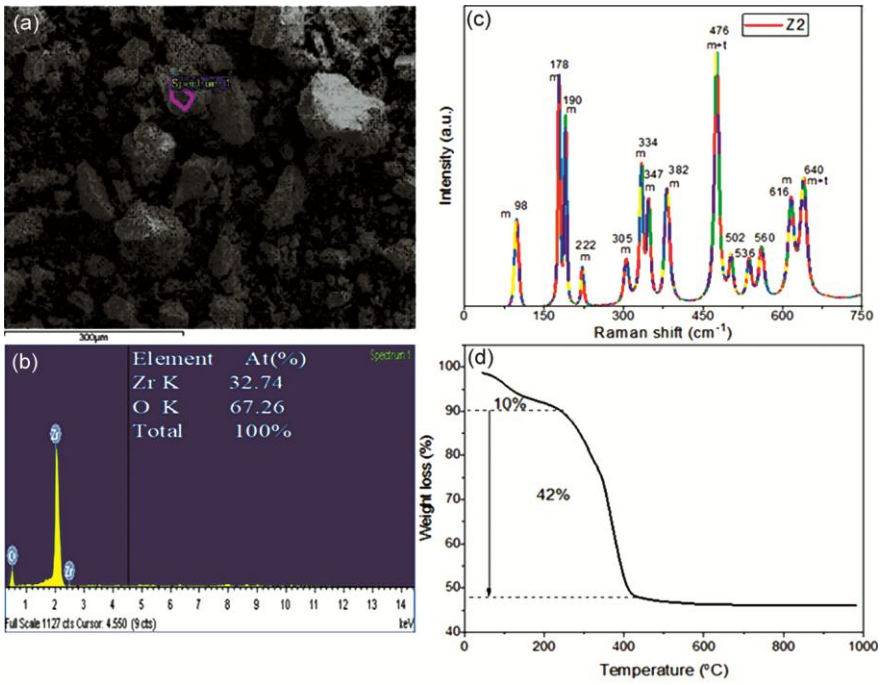

Fig. 4 — (a) SEM image (b) EDX profile (c) Raman spectra of zirconia nanopowders annealed at 850 ºC and (d) TGA curve of as-prepared zirconia powdered sample.

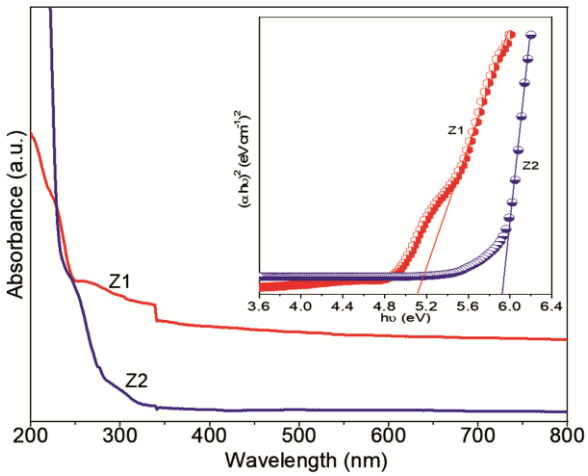

Fig. 5 — Absorbance spectra of zirconia thin films annealed at different temperatures. Inset shows the corresponding Tauc plots.

Table 3 — Raman spectral analysis of zirconia nanopowders annealed at 850 °C

Raman Shift (cm^{-1})	Phase(s)	Raman active mode(s)
98, 180, 190, 305, 347, 560	Monoclinc	A_g
222, 334, 382, 502, 536, 616	Monoclinc	B_g
476	Monoclinc + tetragonal	$A_g + E_g$
640	Monoclinc + tetragonal	$A_g + E_g$

absorption in visible region demonstrating the presence of defects in thin films. The direct allowed band gaps, (Eg ~ 5.1 and 5.9 eV for Z1 and Z2 samples) were determined by extrapolating the straight region of the curves plotted between $(\alpha h\nu)^2$ and hν.

The band gap value increased with temperature, showing the reduction of defects present in films, and the growth of nanocrystalline grains as also confirmed from XRD analysis.

3.7 Photoluminescence

To acquire the knowledge about spectroscopic, electrical and photoelectric properties of materials, photoluminescence study has been performed. PL emission spectra of pure zirconia with different thermal heat treated samples are shown in Fig. 6(a). Emission spectra shows a small peak at 384 nm and a broad band centered at 478 nm, which are both falling in the blue region of E.M. spectra. Peak at 478 nm may be ascribed to transition (O^{2-}) p → d (Zr^{4+})[19]. Appearance of broad band in pure zirconia matrix may be due to oxygen vacancies (V_o). The broadening of peaks occurs due to defects present on the surface or surface roughness of prepared samples due to which the periodicity of lattice breakup.

3.8 CIE co-ordinates and CCT

Chromaticity curve of pure zirconia annealed at 850 °C is shown in Fig. 6(b). The CIE (Commission

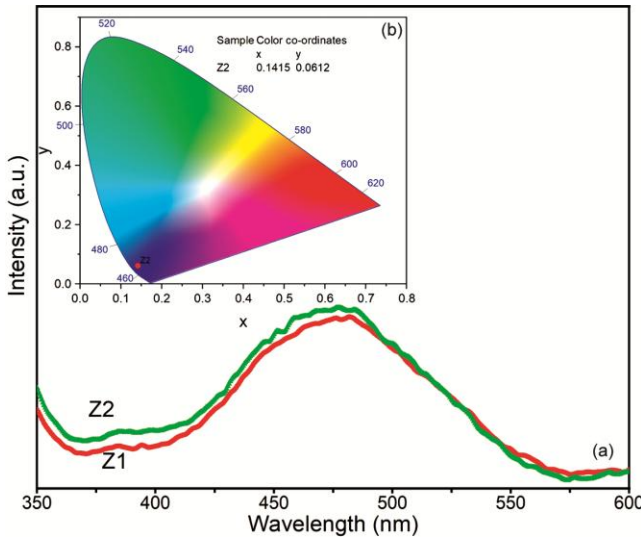

Fig. 6 — (a) PL spectra of zirconia nanopowders annealed at different temperatures, (b) Chromaticity curve of zirconia nanopowder annealed at 850 ^{o}C.

International de I'Eclairage) coordinates x=0.142, y=0.061, fall in blue region of color gamut and is also confirmed by PL spectra. The results indicated that pure zironia can be used in display devices with blue phosphor. The CCT (Correlated Color Temperature) is calculated using CIE co-ordinates and found to be 1883K which is less than 5000K, and hence it can be used as blue light emitter in home appliances.

4 Conclusion

Nanocrystalline zirconia nanoparticles with tetragonal and monoclinic phases were prepared by sol-gel/ spin-coating technique. Presence of these phases was confirmed by XRD, FTIR and Raman studies. Zr and O were present very nearly in stoichiometric ratio as found from EDX spectra. The band gap was increased with temperature, attributed to the reduction of defects presented in the films. PL emission spectra showed a small peak at 384 nm (blue) and a broad band with peak centered at 478nm (blue). Beyond 500 ^{0}C, the formation of crystalline state took place after the removal of impurities presented on the surface of zirconia,. Present studies are beneficial for the assessment of prepared material with regard to fabrication of optoelectronic devices and as blue light emitter in home appliances.

References

1 Schiller S, Heisig U, Goedicke K, Bilz H & Steinfelder K, *Thin Solid Films*, 92(1-2) (1982)81.
2 Niranjan R S, Hwang Y K, Kim D K, Jhung S H, Chang J S & Mulla I S, *Mater Chem Phys*, 92(2-3) (2005) 384.
3 Eguchi K, Setoguchi T, Inoue T& Arai H, *Solid State Ionics*, 52 (1992) 165.
4 HassD D, Groves J F & Wadley H N G, *Surf Coat Technol*, 146 (2001) 85.
5 Graham J L, Almquist C B, Kumar S& Sidhu S,*Catalysis Today*, 88(1-2) (2003)73.
6 Lee S C, Lee J H, Oh T S& Kim Y H,*Sol Energy Mater Sol*, 75(3-4) (2003) 481.
7 Yoshimura M& Somiya S,*JAm Ceram Soc*,(1983) 453.
8 Steele, Brian C & Heinzel A,*Nature* , 414 (6861) (2001) 345.
9 Brailsford A D & Logothetis E M,*Sens Actuators B: Chem*, 52(1-2) (1998) 195.
10 Somov S I, Reinhardt G, Guth U& Gopel W, *Solid State Ionics*, 136 (2000) 137.
11 Stichert W & Schüth F, *Chemistry of Materials*, 10(7) (1998) 2020.
12 Altass H M& Abd El Rahman S K, *J Mol Catal A Chem*, 411 (2016)138.
13 Ding S, Zhao J& Yu Q,*Catalysts*, 9(9) (2019)768.
14 Saruchi S& Kumar S, *Adv Sci Lett*, 20(7-8) (2014) 1558.
15 Jayakumar S, Ananthapadmanabhan P V, Perumal K, Thiyagarajan T K, Mishra S C, Su L T, Tok, A I Y & Guo J, *Mater Sci Eng B*, 176(12)(2011) 894.
16 Cullity B D & Stock S R, Elements of X-ray diffraction (Pearson), 3rd Edn, 2001.
17 Williamson G K & Hall W H,*Acta metallurgica*, 1(1) 1953 22.
18 Jothibas M, Manoharan C, Johnson Jeyakumar S, Praveen P& Joseph Panneerdoss I,*Mater Sci Mater in Electr*, 27(6) (2016) 5851.
19 Lovisa L X, Andres J, Gracia L, Li M S, Paskocimas C A, Bomio M R D, Araújo V D, Longo E& Motta F V, *J Alloys Compd, 695* (2017)3094.